Wei Lv

Patrick E. Phelan

Rajasekaran Swaminathan

School for Engineering of Matter,
Transport and Energy,
Arizona State University,
Tempe, AZ 85287

Todd P. Otanicar

Department of Mechanical Engineering,
The University of Tulsa,
Tulsa, OK 74104

Robert A. Taylor

School of Mechanical and
Manufacturing Engineering,
University of New South Wales,
Sydney, NSW 2032, Australia

Multifunctional Core-Shell Nanoparticle Suspensions for Efficient Absorption

Nanoparticle suspensions are known to offer a variety of benefits for thermal transport and energy conversion. Of particular relevance here are the vast changes to the radiative properties due to the plasmonic nanostructures' large extinction cross section at the corresponding surface plasmon resonance (SPR) wavelength. Recent papers have showed that dielectric core/metallic shell nanoparticles yielded a plasmon resonance wavelength tunable from visible to infrared by changing the ratio of core radius to the total radius. Therefore, we are interested in developing a dispersion of core-shell multifunctional nanoparticles capable of dynamically changing their volume ratio and thus their spectral radiative properties. This paper investigates the surface plasmon resonance effect, wavelength tuning ranges for different metallic shell nanoparticles, and explores the solar-weighted efficiencies of corresponding core-shell nanoparticle suspensions. Through our electrostatic model, we estimate a red-shift in the plasmon resonance peak from a wavelength of about 600 nm to around 1400 nm for Au coated silicon core nanoparticles. Using core-shell nanoparticle dispersions, it is possible to create efficient spectral solar absorption fluids and design materials for applications which require variable spectral absorption or scattering. [DOI: 10.1115/1.4007845]

1 Introduction

Nanofluids, which are liquid nanoparticle suspensions, have attracted numerous investigations that are well summarized in several review articles [1–5]. Nanofluids have been considered for many applications ranging from waste heat removal from a nuclear reactor [6] to medical applications in cancer therapy [7] and solar thermal collectors [8]. Metallic nanoparticles [9] and other plasmonic nanoparticles [10] have the ability to scatter and absorb electromagnetic radiation, enabling their applications with the main thermal transport process of radiation. A solar thermal collector using a dispersion of nanoparticles acting as a direct solar receiver [8,11–13] is one such promising application. In conventional solar thermal collectors, the sunlight is absorbed onto a surface which heats up, then transfers the heat to a working fluid. Direct absorption is a volumetric approach in which radiation is absorbed within a liquid film. This has three distinct advantages over conventional surface-based approaches: first, the absorption of incoming energy in a nanoparticle suspension goes beyond that of surface absorption of a similar material [12], second, the overall thermal resistance can be reduced by reducing the need for convection heat transfer between the absorbing surface and the working fluid [14], and third, the thermal conductivity and convective heat transfer of nanofluids will play a positive role in thermal energy transport.

The radiative properties of nanoparticle suspensions (nanofluids) could have a strong impact on the absorption and emission of energy systems, especially at high temperatures when radiation is important. The main motivation for this study on the radiative control of dispersions is the desire to establish the fundamental knowledge on the ability to control the radiative properties of nanofluids. Another motivation is the potential applications to thermal energy systems. We are attempting to dynamically alter the absorption/emission characteristics, suited to the changing needs of the given application. One such application could be a device that acts as a dual solar thermal collector during the day which could then be transitioned to a radiative cooling system at night (see Fig. 1). This system would enable a much more efficient utilization of space since one system could achieve two objectives instead of requiring two separate systems. It could be applied, for example, in a solar thermal power plant to replace the cooling tower that consumes water. Another possibility is to create a dynamic spectral liquid filter capable of absorbing or transmitting light upon activation.

In this work, we study the potential of nanoparticles for dual absorption/emission characteristics and try to model the best nanostructures whose optical properties can be dramatically altered and dynamically controlled. The choices of the particle material and particle shape are two simple methods to change the spectral properties of nanofluids [10]. Another possible route for tailoring optical properties is through controlling the size of core-shell nanoparticles, for various core and shell materials [15]. Dr. Dai has developed a convenient and effective one-step Pickering emulsion polymerization to synthesize temperature-sensitive core-shell multifunctional nanoparticles [16]. The sizes of this kind core-shell nanoparticles are controlled by the surrounding temperature [16]. Lee et al. [17] recently showed that a mixture of different sized gold nanoshells in aqueous nanofluids will harvest a greater percentage of the solar spectrum than aqueous nanofluids containing solid aluminum nanoparticles, and hence will increase the efficiency of a direct solar receiver. However, for a large scale solar concentrating solar power plant, using gold nanomaterials is likely not an economic choice. In this work, we show that aluminum and copper core-shell nanoparticles suspended in fluids can have an equivalent solar harvesting capacity as their more expensive counterparts—gold and silver.

2 Single Core-Shell Nanoparticle Structure

Figure 2 shows the schematic of a core-shell nanoparticle. In this study, the core is made of a dielectric material (Si), and the shell is made of metallic material (Ag, Au, Al, or Cu). These materials can be changed for the specific absorption and radiation values required. When applying an electromagnetic field, free

Contributed by the Solar Energy Division of ASME for publication in the Journal of Solar Energy Engineering. Manuscript received April 23, 2012; final manuscript received September 23, 2012; published online November 21, 2012. Assoc. Editor: Wojciech Lipinski.

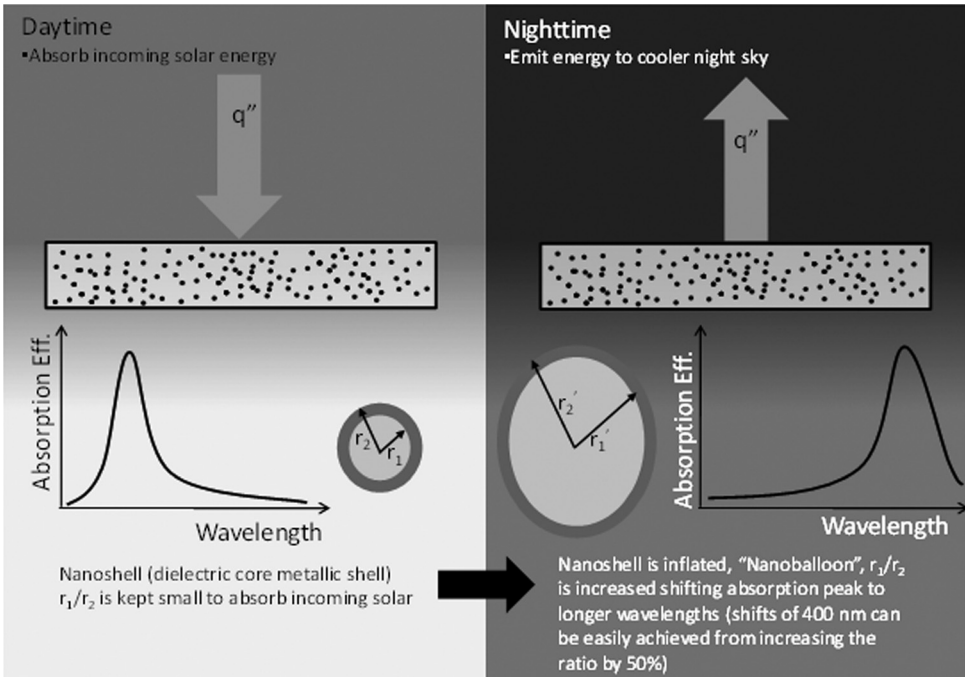

Fig. 1 Dual use solar thermal collector/night sky radiator using core-shell multifunctional nanoparticle suspensions

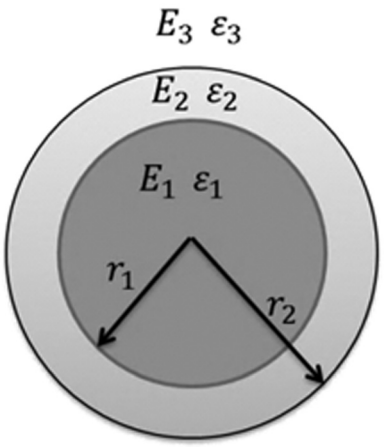

Fig. 2 Core-shell particle geometry; ε_i (1,2,3) are dielectric functions for the core, shell, and embedding regions, r_1, r_2 the core and shell radii and $r_2 - r_1$ the shell thickness. E_i (1,2,3) are the electromagnetic fields in the core, the shell and the embedding media, respectively.

electrons and bound electrons will interact with the field. SPR is caused by the confining force of free conduction electrons. Under specific conditions of wavelength, polarization and incident angle, free electrons (or plasma) at the surface of the nanoparticles absorb incident photons, converting them into surface plasmon waves, which spread across the surface. The large optical polarization associated with the surface plasmon resonance brings on a vast local electric field boost at the nanoparticle surface as well as strongly enhanced light absorption and scattering by the nanoparticle at the SPR frequency [18]. The core-shell nanoparticles' SPR frequency depends on particle size, shape, shell thickness and dielectric properties of the core and surrounding media [9]. In our application, we investigate materials which have a large range of spectral tunability from the visible to the infrared wavelengths.

Various calculations and models have been made on the impact of an electromagnetic field on the spectral and optical properties of core-shell nanoparticles [19–21]. Two assumptions are widely accepted in most models. The first assumption is that the nanoparticle diameter is much smaller than the wavelength of the incident field. There are two major reasons for choosing this small size of nanoparticles. First of all, in a nanofluid-based absorption system, the absorption cross section is more important than the scattering cross section. Although the absorption cross section (C_{abs}) will increase with the particle size, scattering will increase more rapidly, which is not favorable in an independent scattering system. Here, we constrain the scattering cross section (C_{sca}) to be one order of magnitude smaller than the absorption cross section (C_{abs}), $C_{sca}/C_{abs} \leq 0.1$. Although different materials yield different results, this constraint ensures the radius is smaller than 50 nm for most materials. Another important reason for the small size (<50 nm) of the nanoparticle in the nanofluid is for the stability of the dispersion of the nanofluids. Nanoparticles with larger sizes (radius > 100 nm) will fall out of the base fluid due to the gravity. Since most of the incident light from the sun has a wavelength that is at least 10 times larger than the nanoparticle diameter, we can omit higher order terms in the Mie scattering solution and the approximation of Rayleigh scattering ($\pi D/\lambda \ll 1$) is applicable [22]. However, this assumption will not be accurate when the diameter of the core-shell nanoparticle exceeds 50 nm. For larger particles, higher order multipoles, especially quadrupole plasmon resonance should be considered [23]. In this work, the size of core-shell nanoparticles is limited to those smaller than 50 nm. The second assumption is that the incident field does not vary spatially over the diameter of the metallic shell and excitations due to the magnetic field are negligible. If the above two assumptions are appropriate, we can use the so called quasi-static approximation [21].

With the quasi-static approximation, the electric field of the core, shell, and outside region can be calculated from the Laplace equations and specified boundary conditions [24]. The numerical result of the electric field in the core, shell and outside particle can be found in several articles [19,25]. Here, we introduce two effective dielectric functions for convenience [19]

$$\varepsilon_a \equiv \varepsilon_1(3 - 2P) + 2\varepsilon_2 P \tag{1}$$

$$\varepsilon_b \equiv \varepsilon_1 P + \varepsilon_2(3-P) \tag{2}$$

$$P \equiv 1 - (r_1/r_2)^3 \tag{3}$$

where ε_1, ε_2 are dielectric function of core and shell, ε_a, ε_b are the effective dielectric functions, and P is the ratio of shell volume to total particle volume.

For the dielectric core and surrounding dielectric media, we can get the optical properties of bulk material from literature [26]. Since the spectrum ranges from the visible to the infrared region, the imaginary refractive index of surrounding dielectric material cannot be neglected. For example, water and many organic liquids very strongly absorb near-infrared and infrared radiation. For wavelengths $\geq 1.5\,\mu$m, water and organic liquids are generally much better absorbers than most of the nanoparticle materials used in this study. Therefore, we use a wavelength-dependent dielectric function for the dielectric material in the core and embedding media.

The field induced by the composite nanoparticle is equivalent to that of a dipole with the following effective moment [24]:

$$p = \varepsilon_3 \alpha E_0 \tag{4}$$

where α is the polarizability, given here as [19]

$$\alpha = 4\pi r_2^3[(\varepsilon_2\varepsilon_a - \varepsilon_3\varepsilon_b)/(\varepsilon_2\varepsilon_a + 2\varepsilon_3\varepsilon_b)] \tag{5}$$

From this dipole model, one can obtain the analytical expression for the absorption and scattering cross sections [24]

$$C_{\text{sca}} = \frac{k^4}{6\pi}|\alpha|^2 = \frac{128\pi^5}{3\lambda^4}\varepsilon_3^2 r_2^6 \left|\frac{\varepsilon_2\varepsilon_a - \varepsilon_3\varepsilon_b}{\varepsilon_2\varepsilon_a + 2\varepsilon_3\varepsilon_b}\right|^2 \tag{6}$$

$$C_{\text{abs}} = k\,\text{Im}(\alpha) = \frac{8\pi^2\sqrt{\varepsilon_3}}{\lambda} r_2^3\,\text{Im}\left(\frac{\varepsilon_2\varepsilon_a - \varepsilon_3\varepsilon_b}{\varepsilon_2\varepsilon_a + 2\varepsilon_3\varepsilon_b}\right) \tag{7}$$

where $k = \frac{2\pi}{\lambda} n$. Then, we are able to calculate the extinction efficiency of a single nanoparticle by

$$Q_{\text{ext}} = (C_{\text{abs}} + C_{\text{sca}})/\pi r_2^2 \tag{8}$$

We have previously analyzed the optical properties of solar nanofluids based upon solid nanoparticles [27]. After calculation of single-particle extinction efficiency, we can work toward the properties of the total fluid mixture based on the particle concentration. At higher particle concentrations, >0.6% volume fraction, complicated dependent and multiple scattering phenomena can have severe effects since there would be a lot of closely packed particles [28]. It turns out that effective direct solar absorption collection can be achieved for nanofluids of <0.6% volume fraction when the solar collection has sizable absorption path lengths (>1 mm) [27]. Hence, for solar collectors only independent scattering is needed to be considered which makes it easier to analyze the optical properties. When multiple scattering is negligible, the extinction coefficient is calculated from the absorption and scattering efficiencies [24]

$$\sigma_{\text{particle}} = \frac{3 f_v Q_{\text{ext}}}{2D} \tag{9}$$

where D is particle diameter and f_v is the particle volume fraction. After computing the nanoparticles' extinction coefficient in nanofluids, it is necessary to add in the absorption of the base fluid. In this model, we use water as the base fluid since it is a good absorber in the near-infrared and infrared region.

A recent study [27] reported a first-order method to analyze the nanofluids' extinction coefficient, which is found from a simple addition of the base fluid extinction coefficient, σ_{fluid}, and that of all the particles, σ_{particle}

$$\sigma_{\text{nanofluid}} = \sigma_{\text{particle}} + \sigma_{\text{fluid}} \tag{10}$$

where the basefluid extinction coefficient is determined through

$$\sigma_{\text{fluid}} = \frac{4\pi k_{\text{fluid}}}{\lambda} \tag{11}$$

We apply the same approach here, in the results to follow. Classic effective medium theory like Maxwell–Garnet approximation has been used for nanofluids' extinction coefficient modeling and it does not correctly predict the extinction coefficient for nanofluids [27]. Summing the extinction coefficients is much more accurate than the Maxwell–Garnett (MG) effective medium method when comparing to the experiment results. Further work will be necessary to obtain better models for nanoparticle suspensions' optical response.

3 Drude–Lorentz Model and Size Effect

In order to calculate the absorption and scattering cross sections of a core-shell nanoparticle, we need the dielectric function of a metallic shell. From Palik [26] we can get the optical properties of the bulk metallic material. However, the dielectric function of nanoscale metallic particles is size dependent, and can be considerably different from that of the bulk material. Thus, we need to modify the bulk properties to include the impact of size-dependent effects on the nanoparticle optical properties by the Drude–Sommerfeld model. When the dimension of the nanoparticle decreases below the mean free path of the bulk material, the surface causes additional scattering, hence the optical properties need to be modified. This effect has been demonstrated numerically [29], and confirmed experimentally for metallic nanoparticles [21]. The Drude–Sommerfeld model is adapted to model the size effect of metallic nanoparticles using [29]

$$\varepsilon(\omega) = 1 - \omega_p^2 \frac{1}{\omega^2 + i\omega\gamma_{\text{bulk}}} \tag{12}$$

where ω_p is the bulk plasmon frequency, ω is the frequency of the electromagnetic wave, and γ_{bulk} is the relaxation frequency of bulk metal. When the particle size is below the mean free path, the oscillations of the free electrons begin to interact with the particle boundary. This effect results in a modification to the electron decay time $\tau \equiv 1/\gamma$ which is particle size dependent for small particles [30]

$$1/\tau_{\text{eff}} = 1/\tau_0 + AV_f/l_{\text{eff}} \tag{13}$$

where τ_{eff} is the effective relaxation time, τ_0 is the bulk metal free electron scattering time, A is a geometric parameter ranging from 2 to 1 in our model (we assume it to be 1 [29]), V_f is the Fermi velocity, where the experimental value $V_f = 1.38 \times 10^6$ m/s is used for gold nanoparticles [31], and l_{eff} is the effective mean free path used in the determination of the decay time $\tau(l)$. For core-shell nanoparticles, we use a model proposed by Granqvist and Hunderi [32]

$$l_{\text{eff}} = \frac{1}{2}\left[(r_2 - r_1)(r_2^2 - r_1^2)\right]^{1/3} \tag{14}$$

The Drude model itself is sufficient to describe the optical response of most metals below the threshold for interband electron transitions, like aluminum. However, above this threshold, it needs to be coupled with interband absorption which is called the Lorentz model [19]. The Drude and Lorentz model has been experimentally [30] confirmed for gold, silver and copper. The combined Drude and Lorentz model is then [19]

$$\varepsilon(\omega) = \varepsilon(\omega)_{\text{exp}} + \omega_p^2 \frac{1}{\omega^2 + i\omega\gamma_{\text{bulk}}} - \omega_p^2 \frac{1}{\omega^2 + i\omega\gamma(l_{\text{eff}})} \tag{15}$$

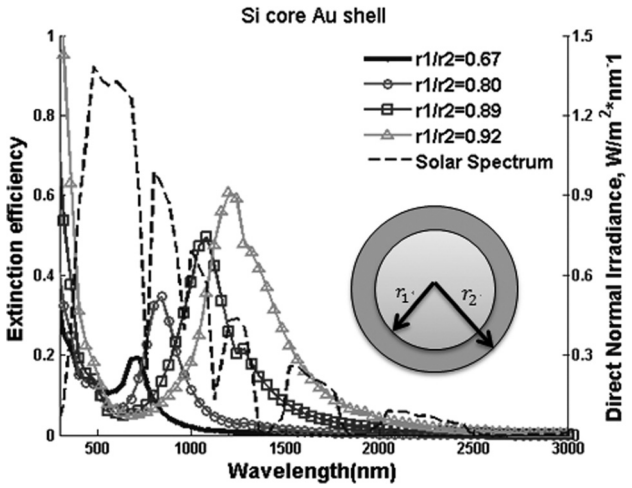

Fig. 3 Individual Si core Au shell core-shell nanoparticle extinction efficiency (shell thickness $r_2 - r_1 = 2$ nm)

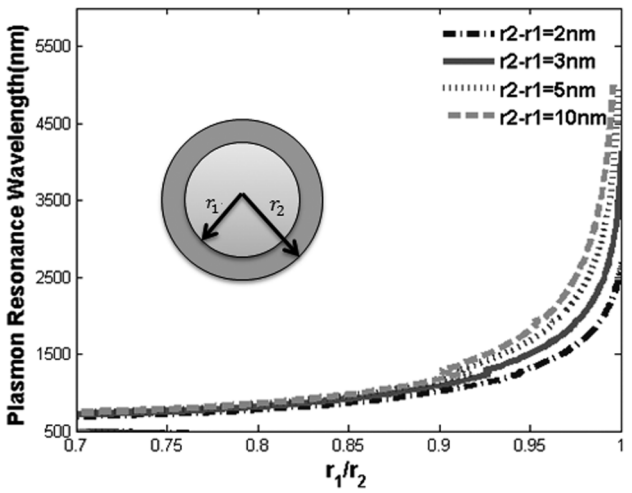

Fig. 4 For Si/Au core-shell nanoparticles, prediction of how the plasmon resonance wavelength varies with the ratio of the core radius to the total radius for shell thicknesses $r_2 - r_1 = 2$, 3, 5, 10 nm

For the dielectric core and surrounding dielectric media, we can use the optical properties from literature [26]. The size effect of the core is neglected since the Si nanoparticles with diameters above 2 nm the dielectric constant equals the bulk value [33].

4 Results and Discussion

4.1 Size Ratio Effect on a Single Particle. Size ratio here means r_1/r_2. Figure 3 shows the potential red-shift effects caused by increasing the size ratio in a single particle. The shell thickness is set to be a constant (2 nm) for modeling simplicity. The total radius r_2 is varied continuously from 6 to 25 nm which keeps the calculations in the Rayleigh regime. The solar spectrum is also plotted to compare with the resonance frequency. From Fig. 3(*a*), reasonable tuning range (approximately 650–1300 nm) is observed. When the size ratio r_1/r_2 increases, the dipole plasmon resonance wavelength shifts to longer wavelengths, which can be explained by Eq. (5), the definition of polarizability. When the denominator of Eq. (5) meets the condition $\varepsilon_2\varepsilon_a = -2\varepsilon_3\varepsilon_b$ at a certain wavelength, metallic dielectric core-shell nanoparticles demonstrate a dipolar plasmon resonance. After plugging Eqs. (1)–(3) into the abovementioned equation, $\varepsilon_2\varepsilon_a = -2\varepsilon_3\varepsilon_b$, it is possible to solve for the dimensionless factor, r_1/r_2, as a function of resonance frequency. For a specified core-shell nanoparticle, the plasmon resonance frequency is a function of the size ratio (if the shell and embedding medium are dielectrics). Then, the following wavelength function is obtained [21]:

$$\frac{r_1}{r_2} = \left[1 + \frac{3}{2}\frac{\varepsilon_2'(\lambda)(\varepsilon_1 + 2\varepsilon_3)}{\varepsilon_2'(\lambda)^2 - \varepsilon_2'(\lambda)(\varepsilon_1 + \varepsilon_3) + \varepsilon_1\varepsilon_3 - \varepsilon_2''(\lambda)^2}\right]^{1/3} \tag{16}$$

where λ is the corresponding plasmon resonance wavelength at a given size ratio r_1/r_2, and $\varepsilon_2'(\lambda)$ and $\varepsilon_2''(\lambda)$ are the real and imaginary parts of the metallic shell dielectric function.

Figure 4 shows the relation between plasmon resonance wavelength λ and the ratio r_1/r_2. The blip at $r_1/r_2 = 0.92$ is caused by the discretization and inaccuracy of experimental dielectric constant data. The ratio of the core radius to the total radius yields a dipolar plasmon resonance peak at a certain frequency. When the ratio increases, the corresponding plasmon $(r_2/(r_2 - r_1) \geq 10)$, the dipolar plasmon resonance frequency of some dielectric core metal shell nanoparticles will shift into the near-infrared, or even to the infrared. From Wien's displacement law, the peak of the radiation emitted at 1000 K occurs at 2.90 μm and at 600 K occurs at 4.83 μm. The surface plasmon resonance wavelength can be tuned to around 5 μm according to Fig. 4. Note that the extinction spectrums of high temperature heat transfer fluids are very different from water and may not be a good absorber and emitter in infrared [34], for example synthetic oils have low absorptance except for several narrow hydrocarbon bands. Hence, using core-shell nanoparticle suspensions could increase the emittance of the fluid medium at high temperature.

This study reveals several core-shell nanoparticle options have plasmon resonance frequencies in the solar spectrum which can also be red-shifted to the infrared—a benefit for thermal emission. Further analysis in the Mie scattering regime will be needed for larger size nanoparticles that have larger r_1/r_2 ratios.

4.2 Extinction Efficiency of Si Core and Metallic (Au, Ag, Cu, Al) Shell Nanoparticles (Shell Thickness $r_2 - r_1 = 3$ nm) Suspended in Water. Numerical calculations have been done on gold and silver, but we also include aluminum and copper since these materials have much long term commercial potential. Table 1 gives the numerical values for bulk electron mean free path, bulk plasmon resonance frequency, and the free electron Fermi velocity for each material. This information enables the bulk metal free electron scattering time to be calculated by the following equation [26]:

$$\tau_0 = l_\infty / V_f \tag{17}$$

where l_∞ is the bulk free electron mean free path. By inserting τ_0 into Eq. (13), the effective scattering time τ_{eff} is easily computed. Inserting the bulk plasma frequency w_p, τ_{eff} and experimentally measured dielectric function of the bulk metal allows us to get the dielectric function of the metallic shell by Eq. (15).

With Eqs. (8)–(11), we are able to model the spectral extinction coefficients of core-shell nanoparticle suspensions. Figure 5 shows the calculation of extinction coefficients for Au shell/Si

Table 1 Bulk mean free path l_∞ of conduction electrons at 273 K, bulk plasma frequency ω_p, and Fermi velocity for potential shell metals [29,30]

Type	Au	Ag	Cu	Al
Bulk mean free path l_∞ (nm)	42	52	42	16
Bulk plasma frequency ω_p (10^{16} Hz)	1.37	1.36	1.64	2.40
Fermi velocity V_f (10^6 m/s)	1.38	1.39	1.57	2.03

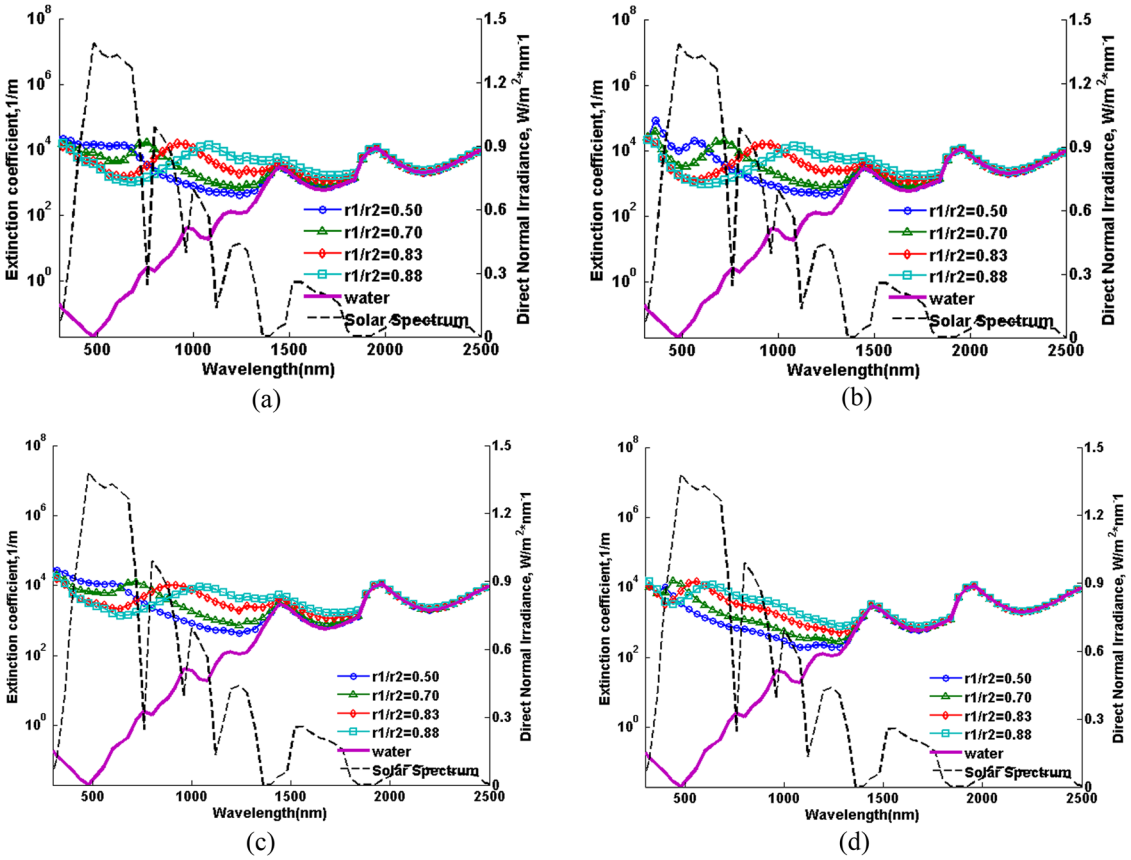

Fig. 5 Extinction coefficients $\sigma_{\text{nanofluid}}$ nanofluid for water-based core-shell nanoparticle suspensions (*a*) Si core/Au shell, (*b*) Si core/Ag shell, (*c*) Si core/Cu shell, and (*d*) Si core/Al shell

core, Ag shell/Si core, Cu shell/Si core and Al shell/Si core nanoparticle suspensions. As discussed above, Au, Ag and Cu have similar single-particle extinction coefficient when the shell thickness is smaller than the free electron mean free path. The solar irradiation spectrum and the extinction coefficient for pure water are also included. Shell thickness of 3 nm is assumed here, since it will have higher extinction efficient in the solar spectrum. The volume fraction is set at $f_v = 0.05\%$. Note that the y-axis of Fig. 5 is on a logarithmic scale.

From Fig. 5, we observe the red-shift of the peak extinction coefficient wavelength as the size ratio increases for all four nanofluids. For comparison, the geometry of the nanoparticle is set to be identical. For silver and copper shell nanoparticle suspensions, they seem to have a similar tuning range as gold, although the bulk optical property is different among gold, silver and copper. In our case, the effective shell thickness is much smaller than the bulk electron mean free path of the metallic materials. Therefore, the dielectric function ε_2 will depend on the shell thickness in our example and result in a difference between the bulk and the nanoscale optical response. This explains why Ag and Cu have similar responses to Au. The tuning range of Si/Al core-shell nanoparticle is smaller than that of the other three. The difference can be deduced from Table 1, as the optical properties of bulk Al are much different from the other three. However, the spectral response of Si/Al nanoparticles fits the solar spectrum quite well. We will see that it results in a relatively high solar-weighted efficiency of a corresponding nanoparticle suspension.

4.3 Solar-Weighted Efficiency Analysis for Selecting the Best Core-Shell Nanoparticle Size and Shell Thickness. Figure 5 gives us a visual impression of how a core-shell nanoparticle increases the extinction coefficient of base fluids. The solar-weighted absorption coefficient A_m, which represents the percentage of solar energy absorbed across a fluid layer of selected thickness [35], can be calculated to quantitatively appreciate the escalation

$$A_m = \frac{\int E_\lambda (1 - e^{-\frac{4\pi k x}{\lambda}}) d\lambda}{\int E_\lambda d\lambda} \tag{18}$$

where E_λ is the solar irradiance per unit wavelength at a certain wavelength, and x is the thickness of the fluid layer, where here we set $x = 1.0$ cm. We set volume fraction to be $f_v = 0.005\%$.

Figure 6 shows the calculated solar-weighted absorption efficiencies of the nanofluids composed of core-shell nanoparticles dispersed in water. It also shows us the dependence of the core radius and shell thickness on the solar-weighted efficiency or in other words, the solar harvesting capacity for different sizes and shell thicknesses for these kinds of nanofluids. The radiative properties of dispersions of nanoparticles are highly volume fraction dependent. The nanofluids' solar-weighted efficiency still rises significantly compared to that of pure water due to the core-shell nanoparticle's radiative response—a large optical cross section at the corresponding surface plasmon wavelength in the visible region. At certain volume fraction, the optical properties of the nanoparticles then become important. The magnitude of the absorption cross section, the bandwidth of the absorption peak and the location of the absorption peak are important for the solar energy harvesting. Figure 6 provides us an intuitive impression on how the core size and shell thickness impact the core-shell nanoparticle suspensions' solar-weighted efficiency. As we discussed above, the optical responses of Au, Ag and Cu nanoparticles are

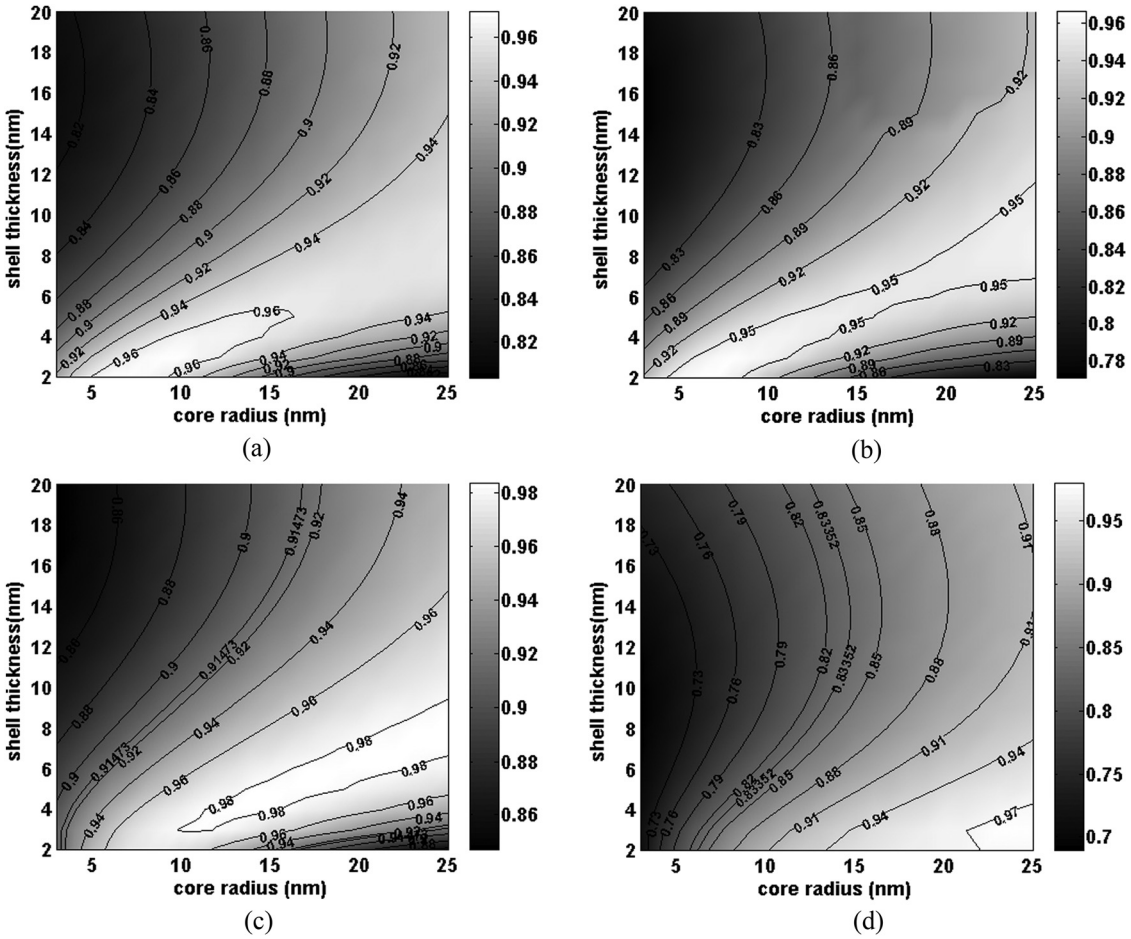

Fig. 6 Contour plot of the solar-weighted efficiency Am for the studied (*a*) Si core/Au shell, (*b*) Si core/Ag shell, (*c*) Si core/Cu shell, and (*d*) Si core/Al shell variant with core radius (3–25 nm), shell thickness (2–20 nm)

Table 2 Solar-weighted absorption coefficient (AM1.5 λ 0.3–2.6 μm $x = 1.0$ cm). $f_v = 0.005\%$

Type	Au	Ag	Cu_1	Cu_2	Al
Core radius (nm)	7	6	11	25	25
Shell thickness (nm)	2	2	3	8	3
Solar-weighted efficiency	0.9714	0.9655	0.9829	0.9829	0.9788
SPR wavelength (nm)	800	760	800	840	640
C_{sca}/C_{abs} at SPR	3.3×10^{-5}	6.4×10^{-5}	8.2×10^{-4}	0.016	0.012

quite similar, which is also reflected in Fig. 6. They all exhibit high solar energy harvesting capacity in the region that have certain size ratio to maintain their absorption peaks around 800 nm. Taking Cu as an example, at a core radius $r_1 = 11$ nm and shell thickness $r_2 - r_1 = 3$ nm, and at a core radius $r_1 = 25$ nm and shell thickness $r_2 - r_1 = 8$ nm, the same solar-weighted efficiency $A_m = 0.9829$ is obtained. As for Al, consistent with the spectra plot Fig. 5(*d*), its absorption peak matches the solar spectrum even at large size ratio (r_1/r_2). The best solar-weighted efficiency for Si/Al core-shell nanoparticle suspensions occurs at large size ratios. Table 2 lists the best solar-weighted efficiency and corresponding geometry of these four different core-shell nanoparticle suspensions. Note: for Cu, it has the exact same highest solar-weighted efficiency at two different geometries.

5 Conclusions

The radiative and optical responses of a dispersion of silicon/metallic core-shell nanoparticles were modeled and compared under several approximations. The motivation of this study is to find nanofluids whose radiative properties can be controlled. Under quasi-static and Rayleigh scattering approximations, the silicon/metal core-shell nanoparticle exhibits a reasonable tuning range of its dipolar surface plasmon resonance frequency. Analysis of the extinction coefficient of four different dielectric core/metallic shell core-shell nanoparticle suspensions and their corresponding solar-weighted efficiency reveals their alterable optical responses and potential for solar energy harvesting. One key conclusion is that core-shell nanoparticles provide the same solar-weighted absorption efficiency in comparison to pure metal nanoparticles with less volume fraction of metal. Taking an 18-nm-radius Au nanoparticle as an example, the same size Si/Au core-shell nanoparticle (2 nm shell thickness) will only need 30% Au by volume, compared with a corresponding solid nanoparticle. Another essential conclusion is that Aluminum and Copper core-shell nanoparticle suspensions can have equivalent or better solar-weighted efficiencies than noble metal core-shell nanoparticle suspensions.

Acknowledgment

The authors gratefully acknowledge support provided by the US National Science Foundation through grants CBET-0932720 and CBET-1066705. We would also like to acknowledge support from the UNSW ECR program.

Nomenclature

A_m = solar-weighted absorption coefficient
C = cross section (m^2)
D = mean particle diameter (nm)
E_λ = spectral solar irradiance (W m^{-2} μm^{-1})
E_i = electric field ($i = 0, 1, 2, 3$)
f_v = volume fraction (%)
l = mean free path (m)
n = real component of refractive index
p = dipole of effective moment
Q = optical efficiency factor
r = particle radius (nm)
V_f = Fermi velocity (m/s)

Greek Symbols

α = polarizability
ε' = real component of dielectric constant, (F/m or kg mm/(mV^2 s^2))
ε'' = imaginary component of dielectric constant (F/m or kg mm/(mV^2 s^2))
λ = wavelength (μm)
σ = extinction coefficient (1/m)
γ = relaxation frequency
∂ = size parameter
τ_0 = free electron scattering time

Subscripts

Abs = absorption
bo = bound electron
bulk = bulk material property
eff = effective
ext = extinction
exp = experimental
sca = scattering
p = plasmon
∞ = bulk material property

References

[1] Wang, X.-Q., and Mujumdar, A. S., 2007, "Heat Transfer Characteristics of Nanofluids: A Review," Int. J. Therm. Sci., **46**(1), pp. 1–19.
[2] Das, S. K., and Choi, S. U. S., 2009, "A Review of Heat Transfer in Nanofluids," Adv. Heat Transfer Nanofluids, **41**(08), pp. 81–197.
[3] Timofeeva, E. V., Yu, W., France, D. M., Singh, D., and Routbort, J. L., 2011, "Nanofluids for Heat Transfer: An Engineering Approach," Nanoscale Res. Lett., **6**(1), p. 182.
[4] Glässl, M., Hilt, M., and Zimmermann, W., 2011, "Convection in Nanofluids With a Particle-Concentration-Dependent Thermal Conductivity," Phys. Rev. E–Stat., Nonlinear Soft Matter Phys., **83**(4 Pt 2), p. 046315.
[5] Taylor, R. A., Phelan, P., Rosengarten, G., Gunawan, A., Lv, W., Otanicar, T., and Prasher, R. S., 2012, "Critical Review of The Novel Applications and Uses of Nanofluids," Proceedings of the 3rd International Conference on Micro/Nanoscale Heat & Mass Transfer, Atlanta, GA, March 3–6, ASME Paper No. MNHMT2012-75189.
[6] Buongiorno, J., Hu, L.-W., Kim, S. J., Hannink, R., Truong, B. A. O., and Forrest, E., 2008, "Nanofluids for Enhanced Economics and Safety of Nuclear Reactors: An Evaluation of the Potential Features, Issues, and Research Gaps," Nucl. Technol., **162**(1), pp. 80–91.
[7] Ferrari, M., 2005, "Cancer Nanotechnology: Opportunities and Challenges," Nat. Rev. Cancer, **5**(3), pp. 161–171.
[8] Tyagi, H., Phelan, P., and Prasher, R. S., 2009, "Predicted Efficiency of a Low-Temperature Nanofluid-Based Direct Absorption Solar Collector," J. Sol. Energy Eng., **131**(4), p. 041004.
[9] Kelly, K. L., Coronado, E., Zhao, L. L., and Schatz, G., 2003, "The Optical Properties of Metal Nanoparticles: The Influence of Size, Shape, and Dielectric Environment," J. Phys. Chem. B, **11**(3), pp. 668–677.
[10] Cole, J. R., and Halas, N. J., 2006, "Optimized Plasmonic Nanoparticle Distributions for Solar Spectrum Harvesting," Appl. Phys. Lett., **89**(15), p. 153120.
[11] Kumar, S., and Tien, C. L., 1990, "Analysis of Combined Radiation and Convection in a Particulate-Laden Liquid Film," J. Sol. Energy Eng., **112**(4), p. 293.
[12] Otanicar, T. P., Phelan, P. E., Prasher, R. S., Rosengarten, G., and Taylor, R. A., 2010, "Nanofluid-Based Direct Absorption Solar Collector," J. Renewable Sustainable Energy, **2**(3), p. 033102.
[13] Lenert, A., and Wang, E. N., 2012, "Optimization of Nanofluid Volumetric Receivers for Solar Thermal Energy Conversion," Sol. Energy, **86**(1), pp. 253–265.
[14] Taylor, R. A., Phelan, P. E., Otanicar, T. P., Walker, C. A., Nguyen, M., Trimble, S., and Prasher, R. S., 2011, "Applicability of Nanofluids in High Flux Solar Collectors," J. Renewable Sustainable Energy, **3**(2), p. 023104.
[15] Halas, N., 2002, "The Optical Properties of Nanoshells," Opt. Photonics News, **13**(8), pp. 26–30.
[16] Ma, H., and Dai, L. L., 2009, "Synthesis of Polystyrene-Silica Composite Particles via One-Step Nanoparticle-Stabilized Emulsion Polymerization," J. Colloid Interface Sci., **333**(2), pp. 807–811.
[17] Lee, B. J., Park, K., Walsh, T., and Xu, L., 2012, "Radiative Heat Transfer Analysis in Plasmonic Nanofluids for Direct Solar Thermal Absorption," J. Sol. Energy Eng., **134**(2), p. 021009.
[18] Jain, P. K., Huang, X., El-Sayed, I. H., and El-Sayed, M. A., 2007, "Review of Some Interesting Surface Plasmon Resonance-Enhanced Properties of Noble Metal Nanoparticles and Their Applications to Biosystems," Plasmonics, **2**(3), pp. 107–118.
[19] Neeves, A. E., and Birnboim, M. H., 1989, "Composite Structures for the Enhancement of Nonlinear-Optical Susceptibility," J. Opt. Soc. Am. B, **6**(4), p. 787–796.
[20] Aden, A. L., and Kerker, M., 1951, "Scattering of Electromagnetic Waves From Two Concentric Spheres," J. Appl. Phys., **22**(1), pp. 1242–1246.
[21] Averitt, R. D., Westcott, S. L., and Halas, N. J., 1999, "Linear Optical Properties of Gold Nanoshells," J. Opt. Soc. Am. B, **16**(10), pp. 1824–1832.
[22] Modest, M. F., 2003, *Radiative Heat Transfer*, 2nd ed., Academic Press, New York.
[23] Hao, E., Li, S., Bailey, R. C., Zou, S., Schatz, G. C., and Hupp, J. T., 2004, "Optical Properties of Metal Nanoshells," J. Phys. Chem. B, **108**(4), pp. 1224–1229.
[24] Bohren, C. F., and Huffman, D. R., 1998, *Absorption and Scattering of Light by Small Particles*, Wiley-VCH Verlag GmbH, Weinheim, Germany.
[25] Averitt, R. D., Sarkar, D., and Halas, N. J., 1997, "Plasmon Resonance Shifts of Au-Coated Au_2S Nanoshells: Insight into Multicomponent Nanoparticle Growth," Phys. Rev. Lett., **78**(22), pp. 4217–4220.
[26] Palik, E. D., 1985, *Handbook of Optical Constants of Solids*, Academic Press, New York.
[27] Taylor, R. A., Phelan, P. E., Otanicar, T. P., Adrian, R. J., and Prasher, R. S., 2011, "Nanofluid Optical Property Characterization: Towards Efficient Direct Absorption Solar Collectors," Nanoscale Res. Lett., **6**(1), p. 225.
[28] Prasher, R. S., 2007, "Thermal Radiation in Dense Nano- and Microparticulate Media," J. Appl. Phys., **102**(7), p. 074316.
[29] Kreibig, U., and Vollmer, V., 1995, *Optical Properties of Metal Clusters* (Springer Series in Materials Science), Springer, Berlin.
[30] Johnson, P. B., and Christy, R. W., 1972, "Optical Constants of Noble Metals," Phys. Rev. B, **6**(12), pp. 4370–4379.
[31] Kittel, C., 1986, *Introduction to Solid State Physics*, Wiley, New York.
[32] Schelm, S., and Smith, G. B., 2005, "Evaluation of the Limits of Resonance Tunability in Metallic Nanoshells With a Spectral Averaging Method.," J. Opt. Soc. Am. A Opt. Image Sci. Vis., **22**(7), pp. 1288–1292.
[33] Wang, L., and Zunger, A., 1994, "Dielectric Constants of Silicon Quantum Dots," Phys. Rev. Lett., **73**(7), pp. 1039–1042.
[34] Otanicar, T. P., Phelan, P. E., and Golden, J. S., 2009, "Optical Properties of Liquids for Direct Absorption Solar Thermal Energy Systems," Sol. Energy, **83**(7), pp. 969–977.
[35] Drotning, W., 1978, "Optical Properties of Solar-Absorbing Oxide Particles Suspended in a Molten Salt Heat Transfer Fluid," Sol. Energy, **20**(4), pp. 313–319.